Accepted Manuscript



Behaviour of *n*-alkanes confined between iron oxide surfaces at high pressure and shear rate: A nonequilibrium molecular dynamics study

Sebastián Echeverri Restrepo, Marcel C.P. van Eijk, James P. Ewen

PII: S0301-679X(19)30267-1

DOI: https://doi.org/10.1016/j.triboint.2019.05.008

Reference: JTRI 5768

To appear in: *Tribology International*

Received Date: 11 February 2019

Revised Date: 8 April 2019

Accepted Date: 5 May 2019

Please cite this article as: Restrepo SebastiáEcheverri, van Eijk MCP, Ewen JP, Behaviour of *n*-alkanes confined between iron oxide surfaces at high pressure and shear rate: A nonequilibrium molecular dynamics study, *Tribology International* (2019), doi: https://doi.org/10.1016/j.triboint.2019.05.008.

This is a PDF file of an unedited manuscript that has been accepted for publication. As a service to our customers we are providing this early version of the manuscript. The manuscript will undergo copyediting, typesetting, and review of the resulting proof before it is published in its final form. Please note that during the production process errors may be discovered which could affect the content, and all legal disclaimers that apply to the journal pertain.

ACCEPTED MANUSCRIPT

Behaviour of n-Alkanes Confined between Iron Oxide Surfaces at High Pressure and Shear Rate: A Nonequilibrium Molecular Dynamics Study

Sebastián Echeverri Restrepo[a,b], Marcel C. P. van Eijk[a], James P. Ewen[c,d]

[a] *SKF Research & Technology Development, PO Box 2350, 3430 DT Nieuwegein, The Netherlands*
[b] *Department of Physics, King's College London, Strand, London WC2R 2LS, UK*
[c] *Department of Mechanical Engineering, Imperial College London, London SW7 2AZ, England, UK*
[d] *Corresponding author*

Abstract

The behaviour of n-alkanes confined and sheared between iron oxide surfaces has been studied using nonequilibrium molecular dynamics simulations. The molecular extension, orientation, film structure, flow, and friction have been investigated for a range of n-alkanes chain lengths under conditions representative of the elastohydrodynamic lubrication regime. At high pressure, the molecules show strong layering and long-range order, suggesting solid-like films. Conversely, high shear rates result in less elongated, layered, and ordered molecules; indicating more liquid-like films. Although Couette flow is usually observed for short n-alkanes, the flow is often non-linear for long n-alkanes. The friction coefficient increases logarithmically with shear rate, but the slope decreases with increasing pressure such that it becomes insensitive to shear rate for long n-alkanes.

1. Introduction

A detailed understanding of the molecular-scale behaviour of fluids confined, pressurised, and sheared between solid surfaces is critical in tribology. Most of the friction losses in lubricated machine components based on elements that roll and slide together (e.g. rolling bearings, gears, constant velocity joints and cam/follower systems) are in the elastohydrodynamic lubrication (EHL) regime. In the EHL regime, thin lubricant films (nm) are subjected to very high pressures (GPa) and shear rates ($> 10^7$ s^{-1}). These conditions are extremely challenging to probe directly through experiment, and thus the behaviour of lubricants under EHL conditions remains somewhat unclear [1].

Alongside experiments, nonequilibrium molecular dynamics (NEMD) simulations can provide unique insights into the behaviour of lubricants under EHL conditions [2]. Since the early 1990s, many studies have investigated the behaviour of lubricants strongly confined (< 6 molecular layers) between solid surfaces, where the effective viscosity is increased relative to the bulk [3]. Early NEMD simulations of thin fluid films suggested that this viscosity increase was due to crystallization for atomic fluids and vitrification for molecular fluids [4]. MD simulations of n-dodecane (C_{12}) showed a transition from liquidlike to solidlike behaviour between 6 and 7 molecular layers at ambient temperature and pressure [5]. Further MD simulations of C_{12} suggested that the initial increase in effective viscosity from confinement was due to the formation of crystal bridges between the surfaces, which was followed by a further increase due to tetratic order throughout the film upon increasing confinement [6, 7].

NEMD simulations of strongly confined systems showed flow behaviour that deviated from the linear (Couette) case, such as boundary slip at the solid surfaces, as well as slip between molecular layers within the fluid film itself [8]. NEMD comparisons between thin (8 molecular layers) films of different n-alkane chain lengths (C_6-C_{80}) suggested that, at low pressure (0.1 MPa), interlayer slip within the ordered film occurred and shear stress was sensitive to the chain length [9]. Conversely, at high pressure (100 MPa), boundary slip occurred and the shear stress was insensitive to the chain length [9]. For thin n-alkane films at high pressure (500 MPa) between α-Fe_2O_3 surfaces, where no slip occurred, the shear stress was shown to be dependent on chain length (C_1-C_{25}) [10]. The shear stress was also dependant on chain length (C_{20}-C_{1400}) for thin (7 molecular layers) n-alkane films sheared between polymer-like surfaces at low pressure (10 MPa), where no slip occurred [11]. However, for metal-like surfaces, upon which the n-alkanes showed slip, the shear stress was independent on the chain length under the same conditions [11]. For the same systems, the shear stress was also shown to increase monotonically with the sliding velocity for metal-like surfaces but to be independent of sliding velocity on polymer-like surfaces [12]. It was also found that shorter (C_{20}) confined n-alkanes melted at high temperatures (0-900 K), whereas longer chains (C_{100}, C_{1400}) only showed thermal softening [13].

Email addresses: sebastian.echeverri.restrepo@skf.com (Sebastián Echeverri Restrepo), marcel.van.eijk@skf.com (Marcel C. P. van Eijk), j.ewen@imperial.ac.uk (James P. Ewen)

ACCEPTED MANUSCRIPT

Relatively fewer NEMD studies have investigated the behaviour of thicker lubricant films ($\geq$ 10 molecular layers) of direct relevance to EHL. Both NEMD simulations [4, 14] and experiments [15] have suggested that there could be similarities between the behaviour of strongly confined films and thicker films subjected to high pressures. Indeed, comprehensive NEMD simulations of relatively thick (35 atomic layers) atomic fluid films showed a range of 'nonequilibrium phases' under high shear rate and pressure conditions. [16, 17] This behaviour was reminiscent of previous observations for more strongly confined films at lower pressure [8]. Further NEMD simulations showed that the nonequilibrium phase transitions observed at high pressure can lead to deviations from classical friction laws [18], which has also been observed for thinner n-alkane films at lower pressure [12]. Recently, unusual friction and nonequilibrium phase behaviour has also been observed in NEMD simulations of relatively thick films of branched and cyclic alkanes under EHL conditions [19, 20, 21]. To design new lubricant molecules to control EHL friction, a clear understanding of how molecular structure affects molecular-scale structure, flow and friction is required.

In this study, the behaviour of n-alkane films ($\geq$ 16 molecular layers) confined, pressurised, and sheared between α-Fe_2O_3 surfaces (as a model for steel) has been investigated under EHL conditions using NEMD simulations. The effect of n-alkane chain length (C_{16}-C_{60}), applied pressure (0.5–1.5 GPa) and shear rate (10^9–10^{10} s^{-1}) on the chain extension and orientation, film structure and flow, and friction has been studied simultaneously. These results increase our understanding of the molecular-scale behaviour of model lubricants under EHL conditions.

2. Methodology

Classical MD simulations were performed using the large-scale atomic/molecular massively parallel simulator (LAMMPS) software [22]. The velocity-Verlet algorithm was used to integrate the equations of motion with a time-step of 1.0 fs. All of the initial configurations were generated using the LAMMPS_builder software [23, 24], which utilises Moltemplate [25] and the Atomic Simulation Environment (ASE) [26]. The systems consist of two parallel atomically-smooth surfaces separated an approximately 8 nm thick n-alkane lubricant layer, as shown in Figure 1. The n-alkane layer was sufficiently thick ($\geq$ 16 molecular layers) such that the lubricant was not strongly layered in the middle of the film and thus any confinement-induced viscosity increase was expected to be negligible [27, 28]. Periodic boundary conditions were applied in the x and y directions.

The lubricant layer consisted of n-alkanes of different lengths: n-hexadecane (C_{16}), n-triacontane (C_{30}) and n-hexacontane (C_{60}). In all cases, a total number of 19200 carbon atoms were inserted; this corresponds to 1200, 640 and 320 molecules for C_{16}, C_{30}, and C_{60}, respectively. In modern lubricants, most base oil molecules are towards the middle of this range, with n-alkanes constituting a large proportion of the various isomers present [29].

For the n-alkane molecules, bonded (bond stretching, angle bending, dihedral torsion) and non-bonded (Lennard-Jones and partial charge) parameters from the long hydrocarbon-optimised potentials for liquid simulations, all-atom force field (L-OPLS-AA) [30, 31] were used. This force-field has been shown to correctly describe the viscous behaviour of long alkanes under ambient and high temperature, high pressure conditions [32]. Moreover, all-atom force-fields have also been shown to be necessary to accurately model phase transitions in confined alkane systems [33]. All C-H bonds were constrained using the SHAKE algorithm [34].

Hematite (α-Fe_2O_3) surfaces were chosen as a representative model for steel surfaces [35]. The hematite surfaces [36] were cleaved and oriented such that the [100] plane is in contact with the lubricant (see Figure 1). The thickness of the surfaces in the z direction is 13.7 Å and the size of the surface in the x and y directions are 80.5 Å and 78.4 Å respectively. The cell dimensions were large enough to prevent the interaction of individual n-alkane chains with their own periodic image under shear. The Fe and O surface atoms are restrained in the corundum crystal structure [36] with harmonic bonds between atoms within 3 Å. The force constant of these bonds was 130 kcal mol^{-1} $Å^{-2}$, which has been shown previously to yield realistic surface rigidity and thermostat efficiency [37].

Surface-lubricant interactions were represented with the Lennard-Jones and Coulombic potentials. The parameters for the Fe and O surface atoms, which determine the strength of the interactions with the lubricant atoms, were taken from Ref. [10] and Ref. [37] respectively. These parameters were developed to reproduce experimental desorption energies of n-alkanes on hematite surfaces. [10] Cross-interactions were evaluated using the geometric mean mixing rules [30]. Lennard-Jones interactions were cut off at 12 Å and electrostatic interactions were evaluated using a slab implementation of the particle-particle-particle-mesh algorithm [38] with a relative accuracy in the forces of 1×10^{-7}.

2.1. Equilibration

First, n-alkane molecules were inserted between the surfaces in an ordered fashion, which was followed by energy minimisation. Next, a properly equilibrated system was a generated using a simple heat-quench sequence. Here, the artificially ordered n-alkane molecules were heated to 2000 K to accelerate diffusion, and left to equilibrate for 10 ns. The system was then quenched back to the target temperature 353 K over a further 10 ns. During the heat-quench sequence, the fluid temperature was controlled using a global Langevin thermostat [39] acting in all Cartesian directions, using a damping constant of 0.1 ps.

Three different criteria were considered to ensure that the systems were well equilibrated. It was verified that the mean square end-to-end distance, $\langle R_{ete}^2 \rangle$, and the mean

square radius of gyration ($< R_g^2 \rangle$ reached a steady state [40]. Long n-alkanes which are not properly equilibrated can present deformation on short length scales that can only be relaxed after the chains have moved a distance equivalent to their own length [41]. In order to ensure that this occurred during equlibration, the mean-squared displacement for the C atoms ($\mathrm{MSD_{atom}}$) and for the centre of mass of the alkane chains ($\mathrm{MSD_{molec}}$) were also monitored during the equilibration. More details regarding the equilibration procedure can be found in the Appendix. The final equilibrated configurations were used as inputs for the compression and shear simulations.

2.2. Compression

After the systems were equilibrated, the pressure was increased by assigning a constant normal (z) force to the outer layer of Fe atoms in the top surface while keeping the outer layer of atoms in the bottom surface fixed in the z direction (see Figure 1). Three different pressure values were considered; 0.5 GPa, 1.0 GPa, and 1.5 GPa. These pressures are of direct relevance to lubricants in the the EHL regime [1].

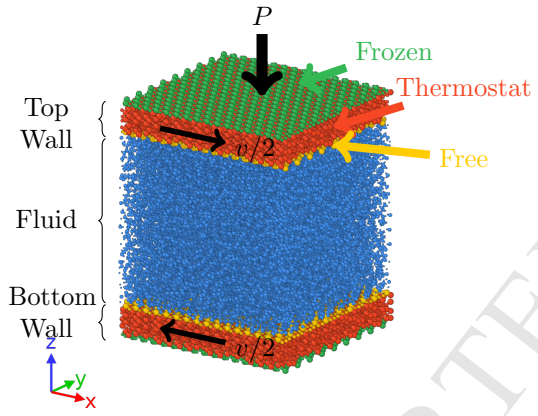


Figure 1: Structure and regions of a representative system for these simulations. The system is divided in three regions, namely, the n-alkane fluid, and the top and bottom surfaces. Within each surface, the *frozen* atoms (green) are used to apply the shearing and compressive constraints, and the *thermostat* atoms (orange) to control the temperature. Both the *free* layers (yellow) and the fluid (blue) atoms are unconstrained.

For the compression and shear stages, the temperature of the system is controlled (T = 353 K) by a Langevin thermostat [39] with a damping coefficient of 0.1 ps, acting on the middle layer of atoms in both surfaces (*thermostat* in Figure 1). The thermostat was applied only in the direction perpendicular to both the sliding and compression (y). This approach has been shown to be more physically accurate compared to application of the thermostat directly to the confined fluid, which can considerably influence friction and flow behaviour, particularly at high shear rates [42, 43, 44].

The compression phase is performed in two steps; first, the pressure is linearly incremented over 10 ns and then the target pressure is maintained for a further 10 ns. The density of the fluid region and the average pressure both reach a steady state well within the simulation time. The average n-alkane densities over the final 1 ns of the compression phase are presented in Table 1. In agreement with experiments data [45], there is an increase in average density with increasing n-alkane chain length, as well as with increasing pressure.

Table 1: Effect of confined n-alkane chain length and pressure on the average density in the fluid region (1)

	ρ [kg m^{-3}]		
P [GPa] / Chain Length	0.5	1.0	1.5
C_{16}	0.87	0.93	0.98
C_{30}	0.90	0.96	1.00
C_{60}	0.91	0.97	1.01

2.3. Shear

After the n-alkanes are equilibrated at the target pressures (0.5–1.5 GPa), the shear response of the lubricant was studied. A shear velocity gradient was imposed on the system by applying an equal and opposite sliding velocity, $v_x = \pm v_s/2$, to the outermost layer of atoms in each surface (see Figure 1) in the x direction. The following sliding velocities were considered, v_s; 10 m s^{-1}, 20 m s^{-1}, 50 m s^{-1} and 100 m s^{-1}. For the simulated film thickness (approx. 8 nm), these correspond to applied shear rates, $\dot{\gamma}$, of approximately 10^9–10^{10} s^{-1}. While these are above those encountered in real engineering components (10^6–10^8 s^{-1}) [46], lower shear rates do not reach a steady state in the available simulation time for the long n-alkanes studied here [2].

To verify that a nonequilibrium steady state was reached, the change in $\langle R_{ete}^2 \rangle$ [40], $\langle S_2^{xz} \rangle$ [47], and shear stress, σ_{xz} [6], were monitored. Lower sliding velocities require a longer simulation time to reach a steady state (up to 200 ns); however, a similar sliding distance is needed, in agreement with experimental observations [48]. In general, a steady state is reached after a shorter sliding distance for shorter n-alkanes and lower pressures. A representative case is C_{30} at 1.0 GPa, for which the change in $\langle R_{ete}^2 \rangle$, $\langle S_2^{xz} \rangle$, and σ_{xz} with sliding distance are presented at four sliding velocities in Figure 2.

Since the initial configuration is the same for all of the sliding velocities, they all have an initial value of $\langle R_{ete}^2 \rangle = 283\,\text{Å}^2$. After this point, $\langle R_{ete}^2 \rangle$ increases and then asymptotes towards a steady state value. This suggests that the chains generally unfold when shear is applied. The steady state $\langle R_{ete}^2 \rangle$ generally decreases with increasing sliding velocity. This is consistent with previous confined NEMD simulations of long n-alkanes at high shear rates [49].

ACCEPTED MANUSCRIPT

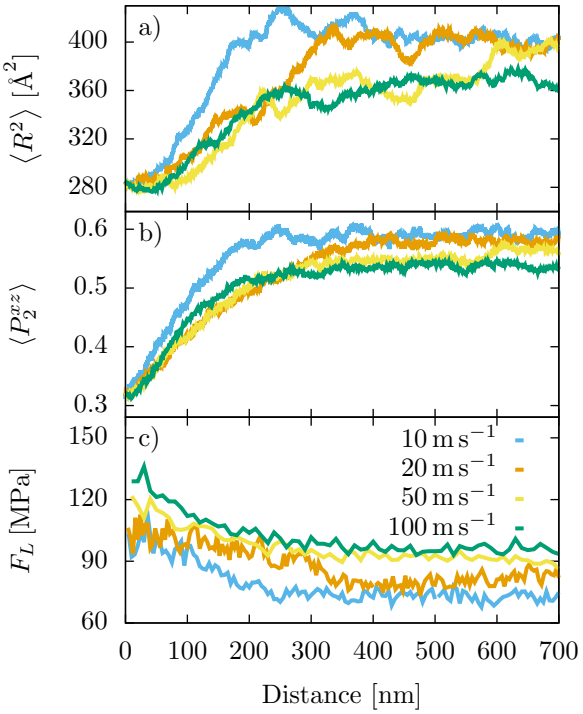


Figure 2: Change in the: a) mean square end-to-end distance, $\langle R^2_{ete} \rangle$, b) average segmental orientation, $\langle S_2^{xz} \rangle$, and c) average shear stress, σ_{xz}, with sliding distance for C_{30} at a pressure of 1.0 GPa.

For ideal chains in the bulk, the average segmental orientation, $\langle S_2^{xz} \rangle = 0.25$. This indicates a uniform distribution of the orientation of the chains, which corresponds to an average orientation angle of 45°. When under confinement, n-alkane molecules close to the surfaces tend to align parallel to them [49], meaning that the angle between the chain and the surface is close to zero, and hence $\langle S_2^{xz} \rangle$ increases. In the case of C_{30} at 1.0 GPa, $\langle S_2^{xz} \rangle = 0.32$ before shear is applied (see Figure 2b), indicating that there is already a preferential orientation due to the presence of the confining surfaces. When sliding is initiated, the chains begin to align with the flow direction, further increasing $\langle S_2^{xz} \rangle$. Generally, $\langle S_2^{xz} \rangle$ decreases with increasing sliding velocity, this is discussed in the next section.

The shear stress, σ_{xz}, is monitored through the average friction force acting on the outermost layer of atoms (frozen atoms in Figure 1) in the top and bottom surfaces (divided by the surface area) in response to the fluid. At the onset of sliding, σ_{xz} increases rapidly to reach a maximum value and then decreases before reaching a steady state. This is indicative of 'stress overshoot' behaviour, which is frequently observed in sheared polymer melts [50]. The sliding distance needed for σ_{xz} to reach a steady state is consistent with that needed for $\langle R^2_{ete} \rangle$ and $\langle S_2^{xz} \rangle$ (Figure 2). Thus σ_{xz} reaches a minimum only when the n-alkane molecules extend and align with the flow direction [50]. Generally, σ_{xz} increases with increasing sliding velocity, this is discussed further in the next section.

Once a nonequilibrium steady state is obtained (Figure 2), sliding is continued for a further 5 ns to 20 ns. During the final 2 ns of these production simulations, $\langle R^2_{ete} \rangle$, $\langle S_2^{xz} \rangle$, and σ_{xz} are measured and averaged. These nonequilibrium steady state results are presented and discussed in the next section.

3. Results and Discussion

First, the effect of chain length, pressure, and shear rate on the chain extension, $\langle R^2_{ete} \rangle$ and orientation, $\langle S_2^{xz} \rangle$ are studied in Section 3.1. The change in film structure and flow are investigated through mass density and velocity profiles as well as radial distribution functions in Section 3.2. Finally, the dependency of the friction on the chain length, pressure, and shear rate are presented in Section 3.3.

3.1. Chain extension and orientation

Longer chains will inherently have higher absolute values of $\langle R^2_{ete} \rangle$, so to compare the variation of $\langle R^2_{ete} \rangle$ between the different n-alkanes, the mean square end-to-end distance was normalised *per C-C bond*; $\langle R^2_{ete} \rangle / (N_{\text{bonds}})^2$. This is presented as a function of shear rate for the different chain lengths and pressures studied in Figure 3.

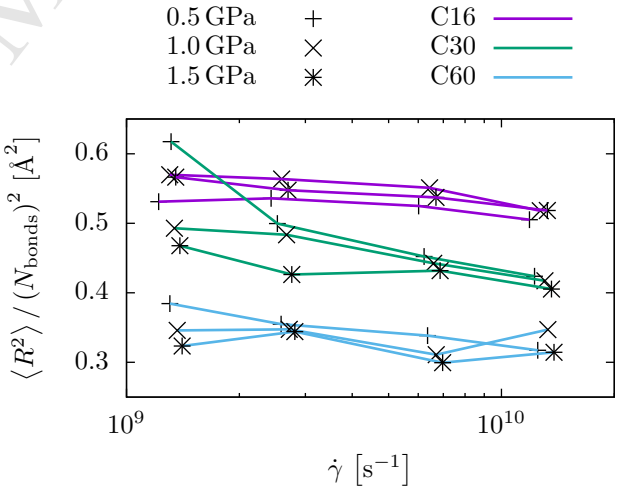


Figure 3: Mean square end-to-end distance, $\langle R^2_{ete} \rangle$ per C-C bond, as a function of the shear rate, $\dot{\gamma}$. Error bars, calculated from the standard deviation between block-averages, are omitted for clarity, but are of a similar size to the symbols.

Figure 3 shows that $\langle R^2_{ete} \rangle / (N_{\text{bonds}})^2$ generally decreases with increasing shear rate, suggesting less extended chain conformations. Previous confined NEMD simulations of thin C_{16} films showed the opposite trend [28]. However, decreasing $\langle R^2_{ete} \rangle$ with increasing shear rate was also observed in confined NEMD simulations of C_{50} at high

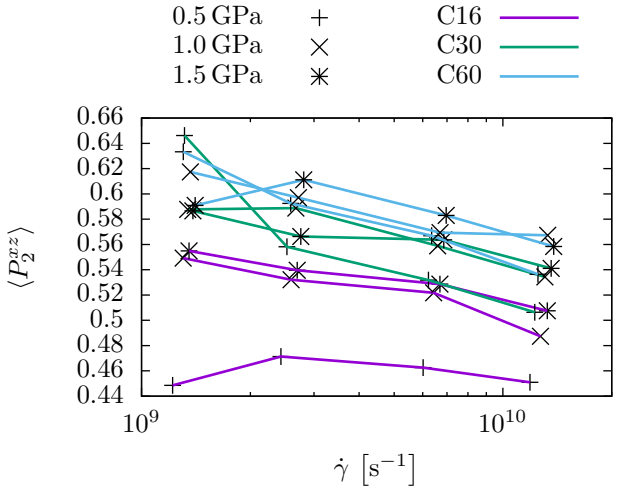


Figure 4: Average segmental orientation, $\langle S_2^{xz} \rangle$, as a function of the shear rate, $\dot{\gamma}$. Error bars, calculated from the standard deviation between block-averages, are omitted for clarity, but are of a similar size to the symbols.

shear rate [49]. This decrease was attributed to strong intermolecular collisions which lead to intense chain rotation and tumbling dynamics at high shear rate [49]. Longer chains (C_{60}) are relatively less extended than shorter chains (C_{16}) at all pressures and shear rates studied. This is expected for *n*-alkanes, even in the absence of confinement and shear [51]. Pressure has a negligible effect on chain extension for the systems and conditions studied here.

Perhaps more surprisingly, Figure 4 shows that there is also a general decrease of $\langle S_2^{xz} \rangle$ with increasing shear rate. This indicates an increase of the average angle of segments relative to the shearing direction at high shear rate (see Appendix), meaning that the chains are relatively less aligned with flow direction. Although such behaviour has also been observed in bulk NEMD simulations of C_{10} at high shear rate [52], the opposite trend is more commonly reported [49, 53, 28]. This discrepancy can be rationalised through the high pressures applied in these simulations which lead to the fluids becoming solid-like; this will be discussed further in the following section. Previous experiments [54] and NEMD simulations [49] have shown that *n*-alkanes close to the confining surfaces align preferentially with the direction of shear (see Appendix). Under the high pressures applied in these NEMD simulations, the ordered region extends further towards the centre of the film (Figure 7), leading to a high value of $\langle S_2^{xz} \rangle$. As the shear rate is increased, the film becomes more liquid-like (Figure 5), and the thickness of the ordered region decreases (Figure 7), meaning that $\langle S_2^{xz} \rangle$ also decreases. The *n*-alkane molecules are generally more aligned at higher pressure, where the solid-like regions are thicker. Consistent with previous bulk NEMD simulations [53], longer *n*-alkanes show more alignment with the shearing direction.

3.2. Film structure and flow

Figure 5 shows the radial distribution function (RDF), $g(r)$ for the C atoms, which was calculated using a cut-off distance of 20 Å. In the calculation of $g(r)$, C atoms separated from each other by one or two C-C bonds were excluded [55].

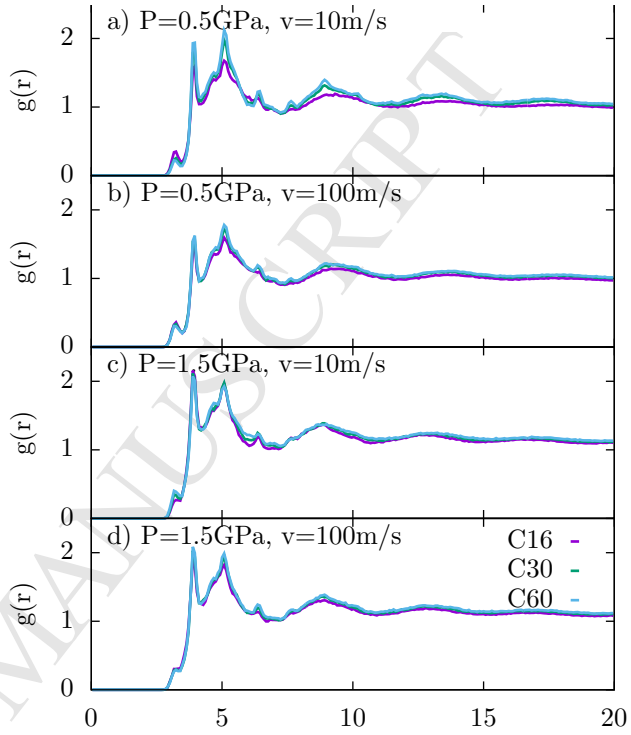


Figure 5: Radial distribution function (RDF), $g(r)$, for C atoms measured during steady state sliding for the three chain lengths studied: C_{16}, C_{30} and C_{60}. a) 0.5 GPa, 10 m s^{-1}, b) 0.5 GPa, 100 m s^{-1}, c) 1.5 GPa, 10 m s^{-1} and d) 1.5 GPa, 100 m s^{-1}.

In Figure 5, three intramolecular $g(r)$ peaks are observed at C-C separations of: $d_1 \approx 3.2$ Å, $d_2 \approx 3.9$ Å and $d_3 \approx 5.1$ Å (see 6). The d_1 and d_2 peaks can be attributed to C atoms separated by three bonds in *gauche* and *trans* conformations respectively [55]. The latter peak is much more intense, indicating that most of the chains are in extended conformations. The d_3 peak is mostly due to C atoms separated by four bonds, and its high intensity further suggests that the chains are in mostly extended conformations. These observations are consistent with the trends shown previously for $\langle R_{ete}^2 \rangle / (N_{\text{bonds}})^2$ (Figure 3). For liquid systems, only one broad intramolecular peak would be expected. The peak splitting in Figure 5 suggests molecular order over different length ranges, which is indicative of glassy systems [55, 56].

There are additional peaks at larger distances in Figure 5, which indicate long-range order and thus crystalline films [57, 58]. These peaks are more intense at higher pressure and lower sliding velocity; suggesting more solid-like

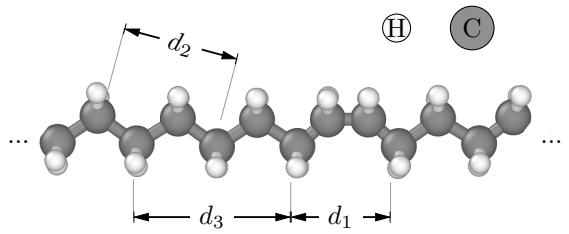


Figure 6: Distances d_1, d_2 and d_3 between pairs of carbon atoms corresponding to the first three peaks of the radial distribution functions for all the systems.

films under these conditions [59]. Moreover, comparing the size of the d_1 and d_2 peaks in Figure 5, it is clear that there is a smaller trans/gauche ratio at high pressure and lower speed, a further indication of more solid-like films under these conditions [60]. The relative peak intensities also suggest that longer chains are more solid-like compared to shorter chains, which is expected from their higher melting points (C_{16} = 291 K, C_{30} = 339 K, C_{60} = 373 K).

Figure 7 shows atomic mass density profiles and x-velocity profiles in the z-dimension for the shortest and longest chains (C_{16}-C_{60}) and lowest and highest pressures (0.5–1.5 GPa) and sliding velocities (10–100 m s^{-1}) studied.

The mass density profiles in Figure 7 show clear molecular layering of the fluids, which is strongest close to the surfaces. Generally, longer chains (C_{60}) show stronger layering compared to shorter chains (C_{16}), suggesting that they form more solid-like films [19]. Comparing Figure 7a with 7b and Figure 7c with 7d, it is clear that the films become less layered, and thus more liquid-like at higher sliding velocity. Comparing Figure 7a with 7c and Figure 7b with 7d, it is also evident that the films become more layered and thus more solid-like at higher pressure.

At the onset of shear, the velocity profiles show deviations from planar Couette flow for several of the systems and conditions studied; however, in most cases, a Couette profile develops once a nonequilibrium steady state is reached (see Appendix). Figure 7 shows steady state velocity profiles for the lowest and highest chain length, pressure, and sliding velocity investigated. At low sliding velocity and low pressure (Figure 7a), the flow for C_{16} remains Couette-like, whereas C_{60} shows some central localisation (CL). CL occurs when the outer solid-like regions of the fluid move at the same velocity as the neighbouring surfaces, and thus only the centre of the film is sheared [16]. The transition from Couette flow to CL has been observed for viscous polymers using in-contact photoluminescence experiments under EHL conditions [61]. It has also been observed in previous NEMD simulations of atomic fluids [16, 17, 18] as well as branched and cyclic alkanes [19, 21] under EHL conditions. At high sliding velocity and low pressure (Figure 7b), Couette flow is maintained for C_{16}. C_{60} also shows a linear velocity profile,

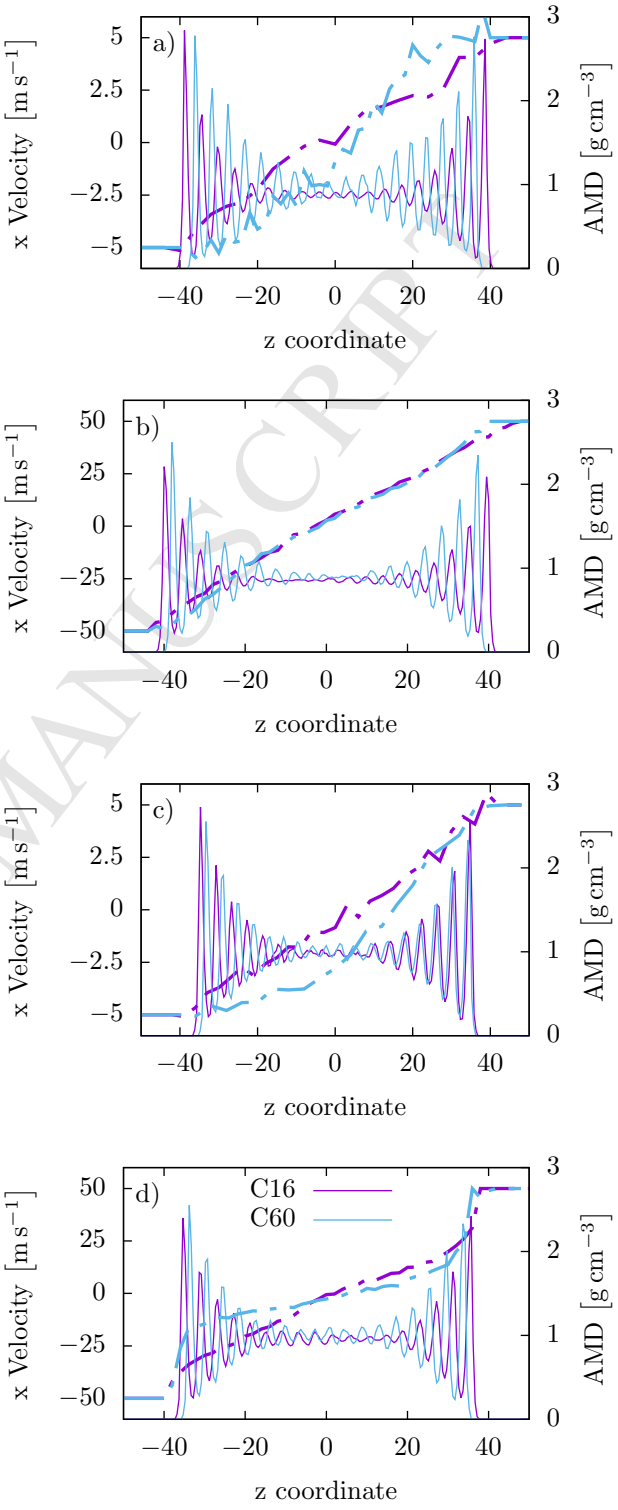


Figure 7: Velocity (solid lines) and atomic mass density (dotted lines) during steady state sliding for two chain lenghts: C_{16} and C_{60}. a) 0.5 GPa, 10 m s^{-1}, b) 0.5 GPa, 100 m s^{-1}, c) 1.5 GPa, 10 m s^{-1} and d) 1.5 GPa, 100 m s^{-1}

but there is a small amount of boundary slip at the fluid-surface interface (slip length ≤ 1 nm). Boundary slip has also been observed in previous NEMD simulations of n-alkane films [62, 12, 63, 20]. However, NEMD of very thick (> 400 nm) C_6 films confined between α-Fe surfaces at 10^5 s^{-1} and 1.0 GPa showed that no boundary slip occurs under such conditions [64]. Atomic-scale roughness has also been shown to reduce boundary slip in confined NEMD simulations [20]. At low sliding velocity and high pressure, (Figure 7c), C_{16} shows Couette flow while C_{60} shows CL. Figure 7d shows that C_{16} also shows slip at high pressure (≈ 10 nm). Moreover, the slip length increases (≈ 40 nm) with increasing pressure for C_{60}, which is consistent with previous NEMD simulations [63] and in-contact photoluminescence experiments [65] of different fluids. The magnitude of the slip lengths are relatively low compared to previous NEMD simulations of n-alkanes [62, 12, 63] due to the wetting α-Fe_2O_3 surfaces [10, 66] and the relatively thick films employed [64]. Overall, larger deviations from Couette flow are observed for longer n-alkanes which form more solid-like films. Under the lower shear rates used experimentally [46], CL is expected for long n-alkanes such as C_{60}, even at rather modest pressure (0.5 GPa).

3.3. Friction

Figure 8 shows that the shear stress, σ_{xz}, increases linearly with increasing pressure, σ_{zz}. This is in agreement with the Derjaguin form of the Amontons-Coulomb friction law; $\sigma_{xz}/\sigma_{zz} = \sigma_0/\sigma_{zz} + \mu$, where σ_{xz} and σ_{zz} are respectively the mean friction force and normal force acting on the outer layer of surface atoms, μ is the friction coefficient, and σ_0 is the load-independent Derjaguin offset [67, 68]. The μ and σ_0 were respectively calculated from the gradient and intercept of the linear fits in Figure 8 for the different systems and conditions studied.

Friction anisotropy, whereby a friction force is detected perpendicular as well as parallel to the sliding direction, has been observed in previous experiments [69] and NEMD simulations [70] of strongly-confined (< 3 layers) n-alkane films. However, friction anisotropy was not observed for the relatively thicker n-alkane films studied here at high pressure.

Figure 9 shows the change in the shear stress, σ_{xz}, with logarithmic shear rate. In general, longer chains give higher σ_{xz} than shorter chains in 9, as expected due to their higher viscosity [71]. This trend has also been observed in previous NEMD simulations of thinner films at lower pressure [9, 11, 12, 10]. The difference in σ_{xz} between chain lengths decreases with increasing shear rate, such that they are very similar at the highest shear rate studied ($\approx 10^{10}\,s^{-1}$). It is important to note that tribological experiments [19, 71] and engineering components [46] operate at lower shear rates than those accessible through NEMD simulations [2]. Thus a larger increase in σ_{xz} with increasing chain length can be expected under these lower shear rates than was observed here. All of the systems undergo shear thinning under the conditions studied, as

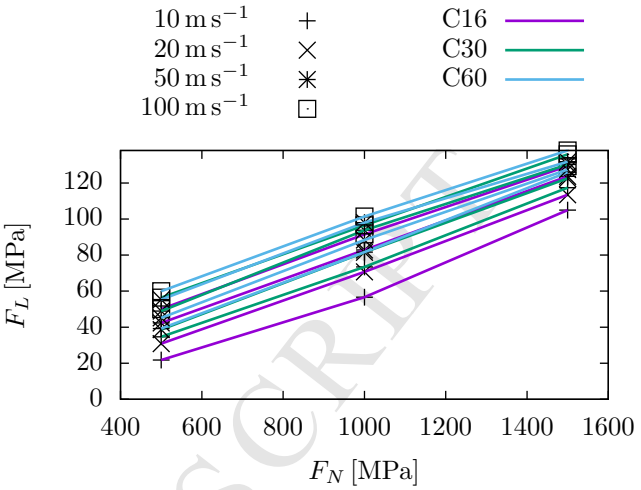


Figure 8: Shear stress, σ_{xz}, as a function of the applied pressure, σ_{zz}, on the outer layer of atoms in the top and bottom surfaces during steady state sliding. Lines represent linear fits to Derjaguin form of the Amontons-Coulomb friction law.

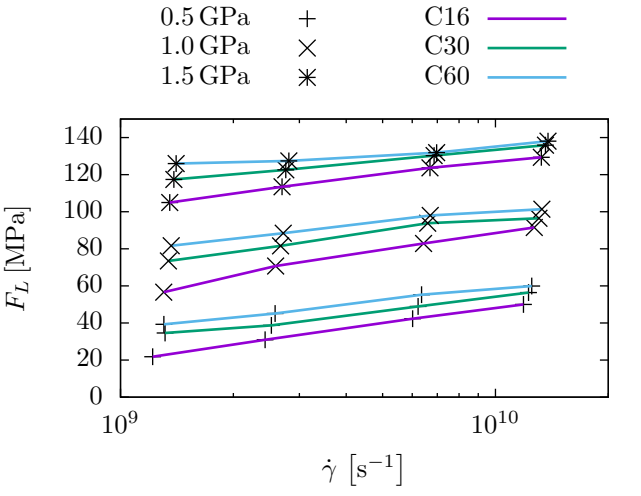


Figure 9: Shear stress, σ_{xz}, versus logarithmic shear rate, $\dot{\gamma}$, during steady state sliding. Error bars, calculated from the standard deviation between the trajectory time-averages, are omitted for clarity, but are of a similar size to the symbols.

shown by the reduction in the effective viscosity, η_{eff}, with increasing shear rate (shown in Appendix) [28, 13, 63].

Generally, σ_{xz} increases linearly with logarithmic shear rate in Figure 9, as is commonly observed for lubricants in macroscopic EHL friction experiments [1, 19]. Similar behaviour has also been reported in previous NEMD simulations of thin (6 molecular layers) C_{20} films between polymer-like surfaces at low pressure (10 MPa) [12]. In Figure 9, the slope of the increase in σ_{xz} with shear rate generally decreases with increasing pressure. This has also been observed in NEMD simulations of both linear [63] and branched [19] alkanes under similar conditions.

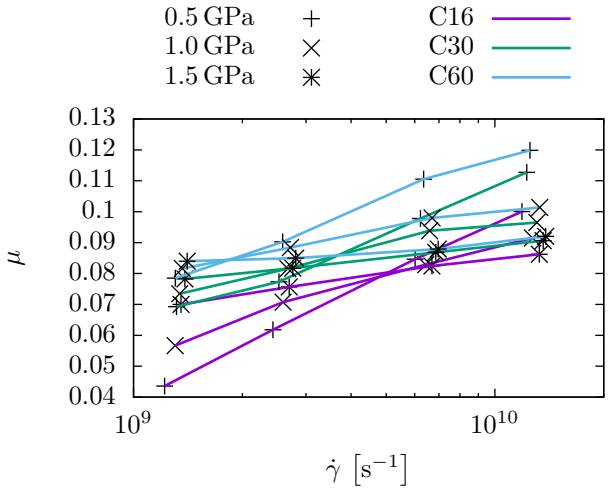


Figure 10: Friction coefficient μ as a function of logarithmic shear rate, $\dot{\gamma}$, during steady state sliding.

Figure 10 and Figure 11 show the change in μ (from gradients of linear fits in Figure 8) and σ_0 (from intercepts of linear fits in Figure 8) with logarithmic shear rate. Unlike branched alkane films [19], most of the n-alkanes show a finite σ_0 in Figure 11, suggesting some adhesion at the solid-liquid interface [68]. Non-zero values of σ_0 have also been obtained from previous NEMD simulations and experiments of a range of confined fluids [72, 67, 68, 73, 24]. Figure 11 shows that σ_0 increases approximately linearly with logarithmic shear rate for all of the n-alkanes studied, in agreement with previous simulations of atomic fluids at high shear rate [72]. In Figure 11, σ_0 is larger for longer n-alkanes, as observed in previous NEMD simulations of n-alkanes (C_{20}-C_{100}) [73]. For short n-alkanes at low shear rate, a negative σ_0 is extrapolated from Figure 8, which was also noted from previous NEMD simulations of atomic fluids [72] and C_{16} [67].

In Figure 10, μ increases linearly with logarithmic shear rate at low pressure (0.5 GPa) for all of the n-alkanes studied. At higher pressure (1.0-1.5 GPa), μ still increases with shear rate for C_{16}, but with a shallower slope. Consequently, at high shear rates, μ is higher at low pressure than at high pressure; an observation that is consis-

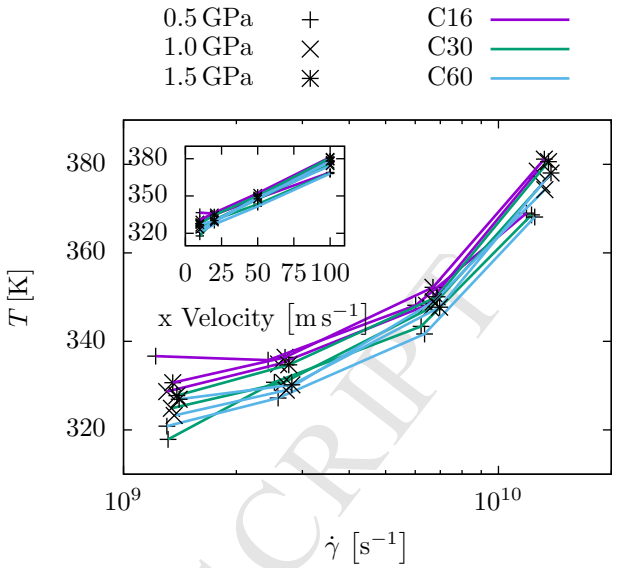


Figure 11: Derjaguin offset, σ_0, versus logarithmic shear rate, $\dot{\gamma}$, during steady state sliding.

tent with previous NEMD simulations of C_{16} [63]. For longer alkanes (C_{30}-C_{60}), μ becomes insensitive to shear rate at high pressure, in line with Coulomb's law for dry friction [67]. The transition to this behaviour, above the limiting shear stress (LSS), has been observed for several fluids in macroscopic friction experiments [74]. It has also been observed for bulky cyclic alkane molecules in NEMD simulations [19, 20]. Similar behaviour has also been reported in previous NEMD simulations of thin C_{60} films between polymer-like surfaces at low pressure (10 MPa) which showed boundary slip [12].

The LSS has been linked to a range of effects, including the glass transition [20] and changes in the flow behaviour [19, 21]. As discussed above, non-linear flow persists into the steady state for some of the systems and conditions studied here (Figure 7). For example, boundary slip occurs at high pressure and shear rate for C_{60} (Figure 7), which has been shown to reduce μ [12]. Moreover, C_{60} also shows CL at low shear rate in Figure 7, whereas shorter n-alkanes remain Couette-like. Interestingly, C_{60} reaches the LSS in Figure 10 at high pressure (1.5 GPa) while C_{16} does not. Since all of the n-alkanes appear glassy (or even crystalline) in Figure 5, these results further support a link between the LSS and non-linear flow behaviour [19, 21].

Severe EHL conditions can lead to large temperature rises within the fluid film as well as at the sliding surfaces [1]. Figure 12 shows the change in average film temperature (details in Appendix) with logarithmic shear rate. At the lowest shear rate studied, the temperature in the fluid region is the same as the thermostatted surfaces (353 K). As predicted by the Archard equation for flash temperature rise [75], there is a linear increase in temper-

ature with increasing sliding velocity (inset in Figure 12). The temperature rise is rather insensitive to chain length and pressure in the ranges studied. Under similar conditions, ΔT is larger than in previous NEMD simulations of thinner n-alkane films [76, 63]. Moreover, the 'critical shear rate' at which a detectable ΔT occurs is lower than in these simulations. This is intuitive because in thicker films, heat generated by the shearing process must travel further before it can be dissipated through the thermostatted surfaces. Indeed, the Archard equation predicts a linear increase in temperature rise with film thickness [75]. The same trend has been observed in recent NEMD simulations of branched and cyclic alkanes [21].

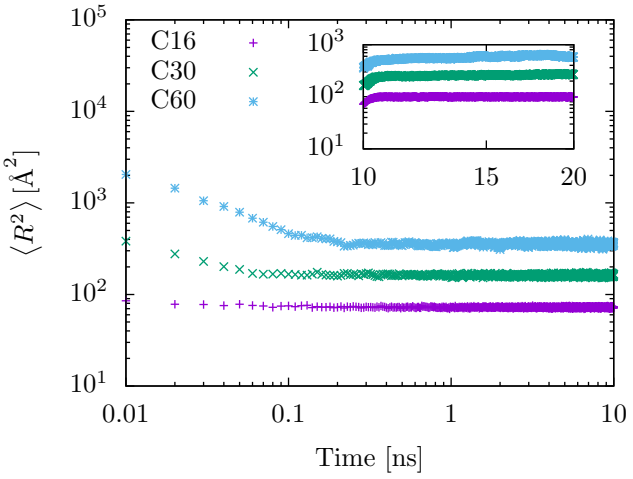


Figure 12: Average temperature rise of the fluid region, ΔT, as a function of logarithmic shear rate, $\dot{\gamma}$. Inset shows the same data versus linear sliding velocity, v_s. Error bars, calculated from the standard deviation between the trajectory time-averages, are omitted for clarity, but are of a similar size to the symbols.

The n-alkane films become more liquid-like at high shear rates, as shown by the reduction in $\langle R^2_{ete} \rangle$ (Figure 3) and $\langle S^{xz}_2 \rangle$ (Figure 4), and long-ranged order (Figure 5). However, even at the highest shear rate and lowest pressure studied here, Figure 5 suggests that all of the n-alkane films remain glassy. This is in agreement with previous NEMD simulations in which only softening rather than melting was observed even at very high temperature (900 K) [13]. The increase of the temperature at high shear rate will decrease the fluid viscosity and also reduce friction. Since the temperature rise increases with increasing shear rate, it might be expected that the LSS behaviour observed for C_{60} at 1.5 GPa could be due to shear heating. However, in Figure 9, the friction coefficient does not increase with shear rate for C_{60} even at low shear rate where there is a negligible ΔT in Figure 12. Therefore the LSS behaviour observed for C_{60} in Figure 9 cannot be attributed purely to shear heating [76, 21].

4. Conclusions

In this study, the behaviour of n-alkane films confined ($\geq$ 16 molecular layers) and sheared between atomically-smooth hematite surfaces under EHL conditions has been investigated using NEMD simulations. The effect of the n-alkane chain length (C_{16}-C_{60}), pressure (0.5-1.5 GPa), and shear rate (10^9-10^{10} s^{-1}) on the chain extension and orientation, film structure and flow, and friction have been studied. An accurate all-atom force-field was used to ensure that the viscosity was close to that expected experimentally.

Starting from ordered chains, a heat-quench cycle was used to equilibrate the systems by monitoring the end-to-end distance and radius of gyration. It was also ensured that the chains moved at least their own size via the mean square displacement. When shear was applied, the end-to-end distance, segmental orientation, and friction were monitored to determine when a nonequilibrium steady state had been reached. The results show that reaching a steady state in n-alkane films depends on the sliding distance rather than the sliding time, in agreement with previous experiments and NEMD simulations.

At high pressure, the films show more layering and ordering in the mass density profiles and RDFs respectively, suggesting that they become more solid-like. Conversely, at higher shear rates, the chains become less elongated, aligned, layered, and ordered; indicating the films become more liquid-like as the fluid film temperature rise increases. Longer n-alkanes are generally more solid-like, in accordance with their higher melting points.

For short n-alkanes, the flow remains mostly Couette-like, but some boundary slip occurs at the highest pressure and shear rate studied. Conversely, long n-alkanes consistently show non-linear flow. At low shear rate, long n-alkanes show central localization, whereby only the middle region of the fluid is sheared. At high shear rate, boundary slip is observed for long n-alkanes, with much larger slip lengths compared to short n-alkanes.

For all of the systems and conditions studied, the shear stress increases linearly with increasing pressure. However, most linear extrapolations of the shear stress to zero pressure showed finite intercepts, suggesting some adhesion. Longer chains, with higher viscosity give higher shear stress, particularly at low shear rates where the films are more solid-like. The shear stress is more sensitive to pressure than to chain length in the ranges studied.

At low pressure, the friction coefficient increases linearly with logarithmic shear rate, as is commonly observed for lubricants in experiments and simulations. For short n-alkanes, the slope of this increase becomes shallower as the pressure increases. For longer n-alkanes, the friction coefficient becomes insensitive to shear rate at high pressure, suggesting that the LSS was reached. A detailed study of the fluid properties reveals that a combination of non-linear flow and shear heating are responsible for this behaviour for the systems and conditions studied here.

ACCEPTED MANUSCRIPT

The results of this study suggest that n-alkanes can show deviations from the commonly assumed flow and friction behaviour at high pressure and shear rate. These deviations are generally larger for longer n-alkanes, which have higher viscosity and melting points.

Acknowledgments

S.E.R. acknowledges the support of the European Commission through the Marie Curie Industry-Academia Partnerships and Pathways (IAPP) iBETTER Project: `http://cordis.europa.eu/project/rcn/109976_en.html`. J.P.E acknowledges the Engineering and Physical Sciences Research Council (EPSRC) for funding via a Doctoral Prize Fellowship and grant EP/P030211/1. The figures showing atomic configurations where generated using the OVITO software [77]. Some of the simulations were facilitated through the Imperial College London Research Computing Service (RCS).

Bibliography

References

[1] H. Spikes and Z. Jie, "History, origins and prediction of elastohydrodynamic friction," *Tribology Letters*, vol. 56, no. 1, pp. 1–25, 2014.

[2] J. P. Ewen, D. M. Heyes, and D. Dini, "Advances in nonequilibrium molecular dynamics simulations of lubricants and additives," *Friction*, vol. 6, no. 4, pp. 349–386, 2018.

[3] S. Granick, "Motions and Relaxations of Confined Liquids," *Science*, vol. 253, no. 5026, pp. 1374–1379, 1991.

[4] P. A. Thompson, G. S. Grest, and M. O. Robbins, "Phase transitions and universal dynamics in confined films," *Physical Review Letters*, vol. 68, no. 23, pp. 3448–3451, 1992.

[5] S. T. Cui, P. T. Cummings, and H. D. Cochran, "Molecular simulation of the transition from liquidlike to solidlike behavior in complex fluids confined to nanoscale gaps," *The Journal of Chemical Physics*, vol. 114, no. 16, pp. 7189–7195, 2001.

[6] A. Jabbarzadeh, P. Harrowell, and R. I. Tanner, "Crystal Bridge Formation Marks the Transition to Rigidity in a Thin Lubrication Film," *Physical Review Letters*, vol. 96, no. 20, p. 206102, 2006.

[7] A. Jabbarzadeh, P. Harrowell, and R. I. Tanner, "Crystal Bridges, Tetratic Order, and Elusive Equilibria: The Role of Structure in Lubrication Films," *The Journal of Physical Chemistry B*, vol. 111, no. 39, pp. 11354–11365, 2007.

[8] P. A. Thompson and M. O. Robbins, "Shear flow near solids: Epitaxial order and flow boundary conditions," *Physical Review A*, vol. 41, no. 12, pp. 6830–6837, 1990.

[9] A. Koike and M. Yoneya, "Chain Length Effects on Frictional Behavior of Confined Ultrathin Films of Linear Alkanes under Shear," *The Journal of Physical Chemistry B*, vol. 102, no. 19, pp. 3669–3675, 1998.

[10] D. Savio, N. Fillot, P. Vergne, and M. Zaccheddu, "A Model for Wall Slip Prediction of Confined n-Alkanes: Effect of Wall-Fluid Interaction Versus Fluid Resistance," *Tribology Letters*, vol. 46, no. 1, pp. 11–22, 2012.

[11] I. M. Sivebaek, V. N. Samoilov, and B. N. J. Persson, "Frictional properties of confined polymers," *The European Physical Journal E*, vol. 27, no. 1, pp. 37–46, 2008.

[12] I. M. Sivebaek, V. N. Samoilov, and B. N. J. Persson, "Velocity Dependence of Friction of Confined Hydrocarbons," *Langmuir*, vol. 26, no. 11, pp. 8721–8728, 2010.

[13] I. M. Sivebaek, V. N. Samoilov, and B. N. J. Persson, "Effective Viscosity of Confined Hydrocarbons," *Physical Review Letters*, vol. 108, no. 3, p. 036102, 2012.

[14] M. O. Robbins and E. D. Smith, "Connecting Molecular-Scale and Macroscopic Tribology †," *Langmuir*, vol. 12, no. 19, pp. 4543–4547, 1996.

[15] J. Van Alsten and S. Granick, "Molecular Tribometry of Ultrathin Liquid Films," *Physical Review Letters*, vol. 61, no. 22, pp. 2570–2573, 1988.

[16] D. M. Heyes, E. R. Smith, D. Dini, H. A. Spikes, and T. A. Zaki, "Pressure dependence of confined liquid behavior subjected to boundary-driven shear," *The Journal of Chemical Physics*, vol. 136, no. 13, p. 134705, 2012.

[17] C. Gattinoni, D. M. Heyes, C. D. Lorenz, and D. Dini, "Traction and nonequilibrium phase behavior of confined sheared liquids at high pressure," *Physical Review E*, vol. 88, no. 5, p. 052406, 2013.

[18] S. Maćkowiak, D. M. Heyes, D. Dini, and A. C. Brańka, "Nonequilibrium phase behavior and friction of confined molecular films under shear: A non-equilibrium molecular dynamics study," *The Journal of Chemical Physics*, vol. 145, no. 16, p. 164704, 2016.

[19] J. P. Ewen, C. Gattinoni, J. Zhang, D. M. Heyes, H. A. Spikes, and D. Dini, "On the effect of confined fluid molecular structure on nonequilibrium phase behaviour and friction," *Physical Chemistry Chemical Physics*, vol. 19, no. 27, pp. 17883–17894, 2017.

[20] A. Porras-Vazquez, L. Martinie, P. Vergne, and N. Fillot, "Independence between friction and velocity distribution in fluids subjected to severe shearing and confinement," *Physical Chemistry Chemical Physics*, vol. 20, no. 43, pp. 27280–27293, 2018.

[21] J. P. Ewen, H. Gao, M. H. Müser, and D. Dini, "Shear heating, flow, and friction of confined molecular fluids at high pressure," *Physical Chemistry Chemical Physics*, vol. 21, no. 10, pp. 5813–5823, 2019.

[22] S. Plimpton, "Fast Parallel Algorithms for Short-Range Molecular Dynamics," *Journal of Computational Physics*, vol. 117, no. 1, pp. 1–19, 1995.

[23] J. P. Ewen and S. Echeverri Restrepo, "LAMMPS_builder, doi.org/10.5281/zenodo.1043868," 2017.

[24] J. P. Ewen, S. Echeverri Restrepo, N. Morgan, and D. Dini, "Nonequilibrium molecular dynamics simulations of stearic acid adsorbed on iron surfaces with nanoscale roughness," *Tribology International*, vol. 107, no. 18, pp. 264–273, 2017.

[25] A. I. Jewett, Z. Zhuang, and J.-E. Shea, "Moltemplate a Coarse-Grained Model Assembly Tool," *Biophysical Journal*, vol. 104, no. 2, p. 169a, 2013.

[26] A. Hjorth Larsen, J. Jørgen Mortensen, J. Blomqvist, I. E. Castelli, R. Christensen, M. Dułak, J. Friis, M. N. Groves, B. Hammer, C. Hargus, E. D. Hermes, P. C. Jennings, P. Bjerre Jensen, J. Kermode, J. R. Kitchin, E. Leonhard Kolsbjerg, J. Kubal, K. Kaasbjerg, S. Lysgaard, J. Bergmann Maronsson, T. Maxson, T. Olsen, L. Pastewka, A. Peterson, C. Rostgaard, J. Schiøtz, O. Schütt, M. Strange, K. S. Thygesen, T. Vegge, L. Vilhelmsen, M. Walter, Z. Zeng, and K. W. Jacobsen, "The atomic simulation environment—a Python library for working with atoms," *Journal of Physics: Condensed Matter*, vol. 29, no. 27, p. 273002, 2017.

[27] M. L. Gee, P. M. McGuiggan, J. N. Israelachvili, and A. M. Homola, "Liquid to solidlike transitions of molecularly thin films under shear," *The Journal of Chemical Physics*, vol. 93, no. 3, pp. 1895–1906, 1990.

[28] A. Jabbarzadeh, J. Atkinson, and R. Tanner, "Nanorheology of molecularly thin films of n-hexadecane in Couette shear flow by molecular dynamics simulation," *Journal of Non-Newtonian Fluid Mechanics*, vol. 77, no. 1-2, pp. 53–78, 1998.

[29] Z. Liang, L. Chen, M. S. Alam, S. Zeraati Rezaei, C. Stark, H. Xu, and R. M. Harrison, "Comprehensive chemical characterization of lubricating oils used in modern vehicular engines utilizing GC × GC-TOFMS," *Fuel*, vol. 220, pp. 792–799, 2018.

[30] W. L. Jorgensen, D. S. Maxwell, and J. Tirado-Rives, "De-

ACCEPTED MANUSCRIPT

velopment and Testing of the OPLS All-Atom Force Field on Conformational Energetics and Properties of Organic Liquids," *Journal of the American Chemical Society*, vol. 118, no. 45, pp. 11225–11236, 1996.

[31] S. W. I. Siu, K. Pluhackova, and R. A. Böckmann, "Optimization of the OPLS-AA Force Field for Long Hydrocarbons," *Journal of Chemical Theory and Computation*, vol. 8, no. 4, pp. 1459–1470, 2012.

[32] J. P. Ewen, C. Gattinoni, F. M. Thakkar, N. Morgan, H. A. Spikes, and D. Dini, "A comparison of classical force-fields for molecular dynamics simulations of lubricants," *Materials*, vol. 9, no. 8, p. 651, 2016.

[33] H. Docherty and P. T. Cummings, "Direct evidence for fluid–solid transition of nanoconfined fluids," *Soft Matter*, vol. 6, no. 8, p. 1640, 2010.

[34] J.-P. Ryckaert, G. Ciccotti, and H. J. Berendsen, "Numerical integration of the cartesian equations of motion of a system with constraints: molecular dynamics of n-alkanes," *Journal of Computational Physics*, vol. 23, no. 3, pp. 327–341, 1977.

[35] S. J. Oh, D. Cook, and H. Townsend, "Characterization of Iron Oxides Commonly Formed as Corrosion Products on Steel," *Hyperfine Interactions*, vol. 112, no. 1/4, pp. 59–66, 1998.

[36] E. N. Maslen, V. A. Streltsov, N. R. Streltsova, and N. Ishizawa, "Synchrotron X-ray study of the electron density in α-Fe 2 O 3," *Acta Crystallographica Section B Structural Science*, vol. 50, no. 4, pp. 435–441, 1994.

[37] H. Berro, N. Fillot, and P. Vergne, "Molecular dynamics simulation of surface energy and ZDDP effects on friction in nano-scale lubricated contacts," *Tribology International*, vol. 43, no. 10, pp. 1811–1822, 2010.

[38] I.-C. Yeh and M. L. Berkowitz, "Ewald summation for systems with slab geometry," *The Journal of Chemical Physics*, vol. 111, no. 7, pp. 3155–3162, 1999.

[39] T. Schneider and E. Stoll, "Molecular-dynamics study of a three-dimensional one-component model for distortive phase transitions," *Physical Review B*, vol. 17, no. 3, pp. 1302–1322, 1978.

[40] D. Brown, J. H. R. Clarke, M. Okuda, and T. Yamazaki, "A molecular dynamics study of chain configurations in n -alkane-like liquids," *The Journal of Chemical Physics*, vol. 100, no. 2, pp. 1684–1692, 1994.

[41] R. Auhl, R. Everaers, G. S. Grest, K. Kremer, and S. J. Plimpton, "Equilibration of long chain polymer melts in computer simulations," *The Journal of Chemical Physics*, vol. 119, no. 24, pp. 12718–12728, 2003.

[42] S. Y. Liem, D. Brown, and J. H. R. Clarke, "Investigation of the homogeneous-shear nonequilibrium-molecular-dynamics method," *Physical Review A*, vol. 45, no. 6, pp. 3706–3713, 1992.

[43] S. Bernardi, B. D. Todd, and D. J. Searles, "Thermostating highly confined fluids," *The Journal of Chemical Physics*, vol. 132, no. 24, p. 244706, 2010.

[44] X. Yong and L. T. Zhang, "Thermostats and thermostat strategies for molecular dynamics simulations of nanofluidics," *The Journal of Chemical Physics*, vol. 138, no. 8, p. 084503, 2013.

[45] K. Griesbaum, A. Behr, D. Biedenkapp, H.-W. Voges, D. Garbe, C. Paetz, G. Collin, D. Mayer, and H. Höke, "Hydrocarbons," in *Ullmann's Encyclopedia of Industrial Chemistry*, Weinheim, Germany: Wiley-VCH Verlag GmbH & Co. KGaA, 2000.

[46] R. I. Taylor, B. R. De Kraker, A. Morina, A. Neville, and T. Liskiewicz, "Shear rates in engines and implications for lubricant design," *Proceedings of the Institution of Mechanical Engineers, Part J: Journal of Engineering Tribology*, vol. 231, no. 9, pp. 1106–1116, 2017.

[47] B. Erman and L. Monnerie, "Theory of segmental orientation in amorphous polymer networks," *Macromolecules*, vol. 18, no. 10, pp. 1985–1991, 1985.

[48] C. Drummond and J. Israelachvili, "Dynamic Behavior of Confined Branched Hydrocarbon Lubricant Fluids under Shear," *Macromolecules*, vol. 33, no. 13, pp. 4910–4920, 2000.

[49] S. Cho, S. Jeong, J. M. Kim, and C. Baig, "Molecular dynamics for linear polymer melts in bulk and confined systems under shear flow," *Scientific Reports*, vol. 7, no. 1, p. 9004, 2017.

[50] S. Jeong, J. M. Kim, and C. Baig, "Effect of Chain Orientation and Stretch on the Stress Overshoot of Entangled Polymeric Materials under Start-Up Shear," *Macromolecules*, vol. 50, no. 8, pp. 3424–3429, 2017.

[51] J. N. Byrd, R. J. Bartlett, and J. A. Montgomery, "At what chain length do unbranched alkanes prefer folded conformations?," *Journal of Physical Chemistry A*, vol. 118, no. 9, pp. 1706–1712, 2014.

[52] P. Padilla and S. Toxvaerd, "Fluid n -decane undergoing planar Couette flow," *The Journal of Chemical Physics*, vol. 97, no. 10, pp. 7687–7694, 1992.

[53] S. T. Cui, S. a. Gupta, P. T. Cummings, and H. D. Cochran, "Molecular dynamics simulations of the rheology of normal decane, hexadecane, and tetracosane," *Journal Of Chemical Physics*, vol. 105, no. 3, pp. 1214–1220, 1996.

[54] C. Drummond, N. Alcantar, and J. Israelachvili, "Shear alignment of confined hydrocarbon liquid films," *Physical Review E*, vol. 66, no. 1, p. 011705, 2002.

[55] M. Bulacu and E. van der Giessen, "Molecular-dynamics simulation study of the glass transition in amorphous polymers with controlled chain stiffness," *Physical Review E*, vol. 76, no. 1, p. 011807, 2007.

[56] I. Valencia-Jaime, C. Desgranges, and J. Delhommelle, "Viscosity of a highly compressed methylated alkane via equilibrium and nonequilibrium molecular dynamics simulations," *Chemical Physics Letters*, vol. 719, pp. 103–109, 2019.

[57] Y. Tsuchiya, H. Hasegawa, and T. Iwatsubo, "Prediction of the melting point of n -alkanes using the molecular dynamics method," *The Journal of Chemical Physics*, vol. 114, no. 5, pp. 2484–2488, 2001.

[58] V. Kalyanasundaram, D. E. Spearot, and A. P. Malshe, "Molecular Dynamics Simulation of Nanoconfinement Induced Organization of n -Decane," *Langmuir*, vol. 25, no. 13, pp. 7553–7560, 2009.

[59] H. Washizu and T. Ohmori, "Molecular dynamics simulations of elastohydrodynamic lubrication oil film," *Lubrication Science*, vol. 22, no. 8, pp. 323–340, 2010.

[60] G. Kavitha and C. Narayana, "Raman Spectroscopic Investigations of Pressure-Induced Phase Transitions in n -Hexane," *The Journal of Physical Chemistry B*, vol. 111, no. 51, pp. 14130–14135, 2007.

[61] B. Galmiche, A. Ponjavic, and J. S. S. Wong, "Flow measurements of a polyphenyl ether oil in an elastohydrodynamic contact," *Journal of Physics: Condensed Matter*, vol. 28, no. 13, p. 134005, 2016.

[62] A. Jabbarzadeh, J. D. Atkinson, and R. I. Tanner, "Wall slip in the molecular dynamics simulation of thin films of hexadecane," *The Journal of Chemical Physics*, vol. 110, no. 5, pp. 2612–2620, 1999.

[63] T. Ta, A. Tieu, H. Zhu, B. Kosasih, Q. Zhu, and H. Phan, "The structural, tribological, and rheological dependency of thin hexadecane film confined between iron and iron oxide surfaces under sliding conditions," *Tribology International*, vol. 113, pp. 26–35, 2017.

[64] H. Washizu, S.-a. Hyodo, T. Ohmori, N. Nishino, and A. Suzuki, "Macroscopic No-Slip Boundary Condition Confirmed in Full Atomistic Simulation of Oil Film," *Tribology Online*, vol. 9, no. 2, pp. 45–50, 2014.

[65] A. Ponjavic and J. S. S. Wong, "The effect of boundary slip on elastohydrodynamic lubrication," *RSC Adv.*, vol. 4, no. 40, pp. 20821–20829, 2014.

[66] D. T. Ta, A. K. Tieu, H. T. Zhu, and B. Kosasih, "Thin film lubrication of hexadecane confined by iron and iron oxide surfaces: A crucial role of surface structure," *The Journal of Chemical Physics*, vol. 143, no. 16, p. 164702, 2015.

[67] J. Gao, W. D. Luedtke, D. Gourdon, M. Ruths, J. N. Israelachvili, and U. Landman, "Frictional Forces and Amontons' Law: From the Molecular to the Macroscopic Scale," *Journal of Physical Chemistry B*, vol. 108, pp. 3410–3425, 2004.

[68] S. J. Eder, A. Vernes, and G. Betz, "On the Derjaguin Offset in Boundary-Lubricated Nanotribological Systems," *Langmuir*, vol. 29, no. 45, pp. 13760–13772, 2013.
[69] K. Kristiansen, X. Banquy, H. Zeng, E. Charrault, S. Giasson, and J. Israelachvili, "Measurements of Anisotropic (Off-Axis) Friction-Induced Motion," *Advanced Materials*, vol. 24, no. 38, pp. 5236–5241, 2012.
[70] A. Jabbarzadeh, "Friction anisotropy in confined alkanes: Linear and branched molecules," *Tribology International*, vol. 97, pp. 108–115, 2016.
[71] J. Zhang, A. Tan, and H. Spikes, "Effect of Base Oil Structure on Elastohydrodynamic Friction," *Tribology Letters*, vol. 65, no. 1, p. 13, 2017.
[72] G. He and M. O. Robbins, "Simulations of the kinetic friction due to adsorbed surface layers," *Tribology Letters*, vol. 10, no. 1-2, pp. 7–14, 2001.
[73] I. M. Sivebaek and B. N. Persson, "Shearing Nanometer-Thick Confined Hydrocarbon Films: Friction and Adhesion," *Tribology Letters*, vol. 62, no. 1, pp. 1–7, 2016.
[74] L. Martinie and P. Vergne, "Lubrication at Extreme Conditions: A Discussion About the Limiting Shear Stress Concept," *Tribology Letters*, vol. 63, no. 2, p. 21, 2016.
[75] J. Archard, "The temperature of rubbing surfaces," *Wear*, vol. 2, no. 6, pp. 438–455, 1959.
[76] H. Berro, N. Fillot, P. Vergne, T. Tokumasu, T. Ohara, and G. Kikugawa, "Energy dissipation in non-isothermal molecular dynamics simulations of confined liquids under shear," *The Journal of Chemical Physics*, vol. 135, no. 13, p. 134708, 2011.
[77] A. Stukowski, "Visualization and analysis of atomistic simulation data with OVITO-the Open Visualization Tool," *Modelling and Simulation in Materials Science and Engineering*, vol. 18, no. 1, p. 015012, 2010.

Appendix A. Definitions

Appendix A.1. Segmental Orientation

$\langle S_2 \rangle$ describes the orientation of the chemical bonds in terms of the second Legendre polynomial [47]:

$$\langle S_2 \rangle = \frac{3\left\langle \cos^2 \alpha \right\rangle - 1}{2}, \tag{A.1}$$

where α is the angle between a chain segment and a reference axis. In practice, $\left\langle \cos^2 \alpha \right\rangle$ is calculated using:

$$\left\langle \cos^2 \alpha \right\rangle = \frac{1}{N_{\text{bonds}}} \sum_{b=1}^{N_{\text{bonds}}} \left(\frac{\mathbf{r}_{ij}^b}{r_{ij}^b} \cdot \hat{\imath} \right)^2 \tag{A.2}$$

in which N_{bonds} is the total number of bonds, $\mathbf{r}_{ij}^b$ is the difference between the positions of the two atoms that form the bond b, and $\hat{\imath}$ is the direction of the main axis.

In this study, the changes of the orientation in the sliding direction are monitored, through the segmental orientation with respect to x projected in the xz plane: $\langle S_2^{xy} \rangle$. Note that, by definition, if all the molecules are parallel to the shearing direction $\langle S_2^{xz} \rangle = 1$; if all the chains are perpendicular to the surfaces $\langle S_2^{xz} \rangle = -0.5$; and if the chains are oriented at 45°, or if they are randomly oriented $\langle S_2^{xz} \rangle = 0.25$

Appendix A.2. End-to-end distance

$\left\langle R_{ete}^2 \right\rangle$ is the mean square of the magnitude of the vector that points from one end of a chain to the other end. For a system containing several chains, the mean square end-to-end distance, $\left\langle R_{ete}^2 \right\rangle$, is given by the following equation [40]:

$$\left\langle R_{ete}^2 \right\rangle = \left\langle \left(\mathbf{r}_1 - \mathbf{r}_N \right)^2 \right\rangle \tag{A.3}$$

where, for each chain, N is the number of atoms and $\mathbf{r}_i$ is the position vector of atom i.

Appendix A.3. Radius of gyration

$\left\langle R_g^2 \right\rangle$ is the mean squared distance of each atom in the n-alkane chain from its centre of mass, as defined in the following equation[40]:

$$\left\langle R_g^2 \right\rangle = \frac{\left\langle \sum_{i=1}^{N} \left(\left\| \mathbf{r}_i - \mathbf{r}_{\text{com}} \right\| \right)^2 \right\rangle}{N} \tag{A.4}$$

where, for each chain, N is the number of atoms, $\mathbf{r}_i$ is the position vector of atom i and $\mathbf{r}_{\text{com}}$ is the centre of mass.

Appendix A.4. Mean squared displacement

The MSD of an atom is a measure of the deviation between its current and its initial position. The MSD is usually averaged over the number of atoms (N) and its slope when plotted over time can be used to quantify the diffusion coefficient [41]. The MSD can be defined as:

$$\text{MSD} = \frac{1}{N} \sum_{i=1}^{N} \left(\mathbf{r}_i\left(t\right) - \mathbf{r}_i\left(0\right) \right)^2 \tag{A.5}$$

where $\mathbf{r}_i\left(t\right)$ is a vector containing the coordinates of atom i at time t.

Appendix A.5. Average film temperature

As common in NEMD simulations, the temperature of the lubricant is calculated via the kinetic energy of the atoms but excluding the velocity component in the direction of sliding (x) to avoid contributions that are not related to the thermal vibration of the atoms [17]. The measurements are block-averaged every 100 fs, the ΔT values shown in Figure 12 are the time-averaged values from the final 1 ns of the sliding phase.

Appendix B. Equilibration

Figure B.13 shows the different stages of the simulation procedure employed here. Starting from an artificially ordered chains, the a heat-quench cycle is used to equilibrate the system, followed by compression and shear. Further details regarding the equilibration are shown below.

The change in $\left\langle R_{ete}^2 \right\rangle$ and $\left\langle R_g^2 \right\rangle$ for C_{16}, C_{30} and C_{60} at 2000 K are presented on the main part of Figures B.14 and B.15. For the case of C_{60}, which has lower diffusivity, these two quantities reach a steady state after approximately 2×10^5 steps (0.2 ns). The insets of the figures show the evolution of the same quantities after reducing the temperature to 353 K; after 1×10^7 steps (10 ns), both

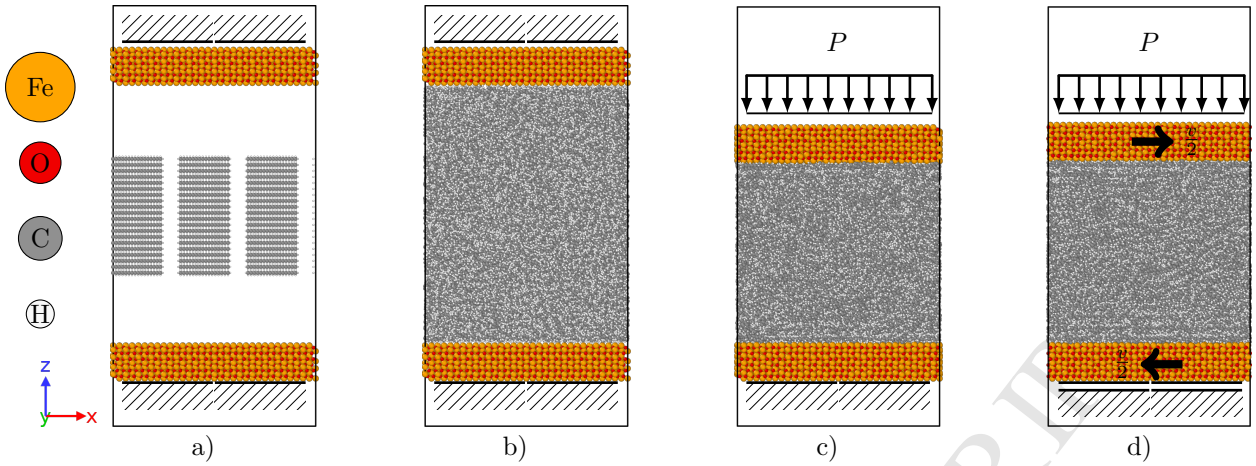


Figure B.13: Steps of the simulation procedure: a) System generation, b) equilibration, c) compression, d) shear. The orange atoms represent iron (Fe), red oxygen (O), gray carbon (C), and white hydrogen (H).

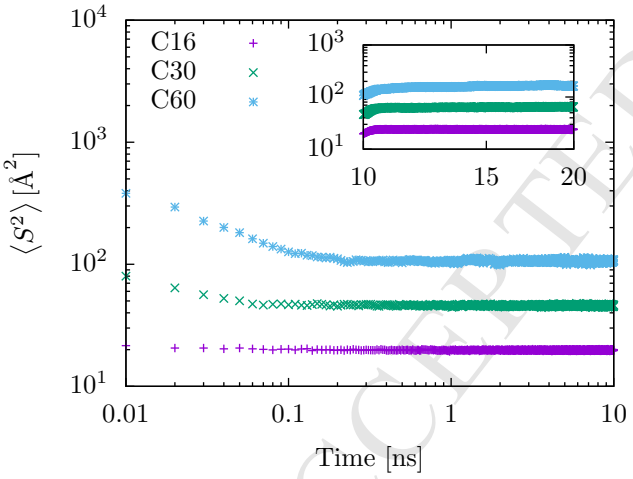


Figure B.14: Mean square end-to-end distance, $\langle R^2_{ete} \rangle$, during the equilibration stage for the three considered alkane lengths: C_{16}, C_{30} and C_{60}. The main plot shows the initial equilibration at 2000 K; the inset the continuation at 353 K.

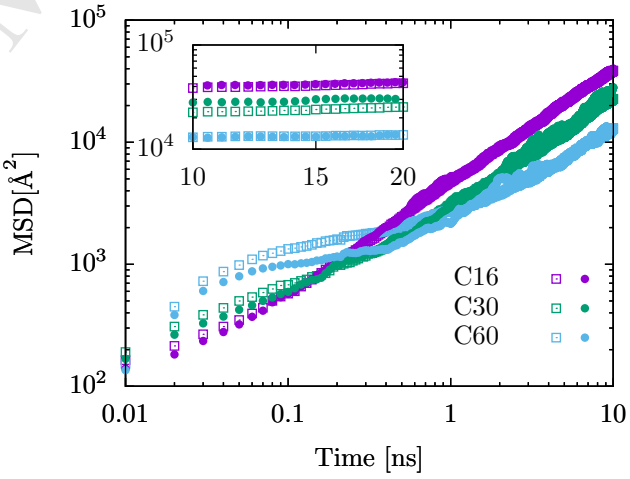


Figure B.15: Mean square radius of gyration, $\langle R^2_g \rangle$, during the equilibration stage for the three considered alkane lengths: C_{16}, C_{30} and C_{60}. The main plot shows the initial equilibration at 2000 K; the inset the continuation at 353 K.

$\langle R^2_{ete} \rangle$ and $\langle R^2_g \rangle$ have reached their equilibrium values for the n-alkanes considered.

The last criterion, is based on the fact that systems of long n-alkanes can present deformation on short length scales that can only be relaxed after the molecules have moved at least their own length [41]. In order to verify this, the mean squared displacement (MSD) for the individual atoms ($\mathrm{MSD_{atom}}$) and for the centre of mass of the n-alkane chains ($\mathrm{MSD_{molec}}$) were followed during equilibration.

Figure B.16 shows the $\mathrm{MSD_{atom}}$ and $\mathrm{MSD_{molec}}$ for the three different systems. The main plot shows the evolution at 2000 K and the inset show the change at 353 K. Note that because the molecules are first introduced into the system in an artificially ordered fashion (see Figure B.13), the diffusivity of the longer chains is initially higher than that of the shorter chains. If we take the length of a C_{60} chain to be ≈ 74 Å (the angle between the C-C bonds is 109.5° and the C-C distance equal to 1.54 Å), the molecules move their own size after $\approx 3 \times 10^6$ to 4×10^6 steps (3 ns to 4 ns). Using a conservative approach, the systems are all equilibrated for 1×10^7 steps (10 ns). The insets show the evolution after the temperature has been decreased; here, as expected, the slope of the $\mathrm{MSD_{atom}}$ and $\mathrm{MSD_{molec}}$ curves is much shallower than at higher temperatures.

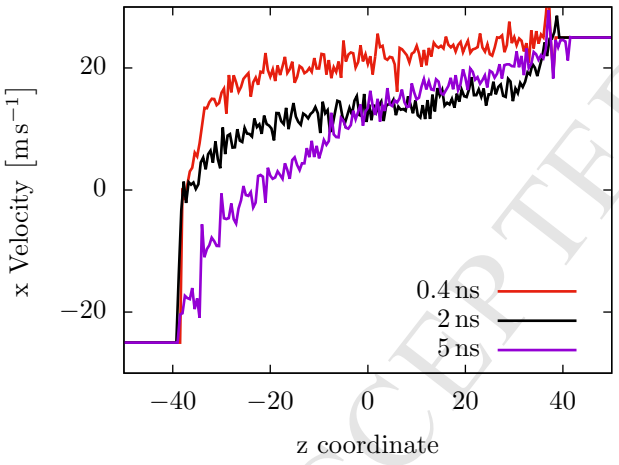


Figure B.16: Mean squared displacement (MSD) during the equilibration stage for the three considered alkane lengths: C_{16}, C_{30} and C_{60}. The main plot shows the initial equilibration at 2000 K; the inset the continuation at 353 K. The full circles represent the mean squared displacement per atom ($\mathrm{MSD_{atom}}$) while the empty squares the mean squared displacement per centre of mass of chain ($\mathrm{MSD_{molec}}$).

Appendix C. Transient Velocity Profiles

A representative example of initial deviations from Couette flow at the onset of sliding is shown for C_{30}, 1.0 GPa and 50 m s^{-1} in Figure C.17. Most systems eventually develop Couette-like profiles, but non-linear flow persists into the steady state for some of the systems and conditions studied (Figure 7).

Figure C.17: Velocity profiles along x at three different times during the transient state of the simulation. Results are presented for the case of C_{30}, 1.0 GPa and 50 m s^{-1}.

Appendix D. Effective Viscosity

The effective viscosity of the lubricant, $\eta_{eff} = (\sigma_{xz}) / (\dot{\gamma})$ [3]. The shear rate was calculated as the ratio of the sliding velocity and the thickness of the fluid region once a nonequilibrium steady state was reached.

Figure D.18 shows the change in η_{eff} with logarithmic shear rate for all the systems studied. As already seen by many other authors, increasing the shear rate results in a reduced η_{eff}, showing that thin films exhibit shear thinning under the high shear rates studied [28, 13, 63]. Only the shortest chain (C_{16}) at the lowest pressure (0.5 GPa) is close to reaching the Newtonian plateau at the lowest shear rate studied 10^9 s^{-1}.

Figure D.18: Effective viscosity, η_{eff}, as a function of the shear rate, $\dot{\gamma}$, measured after reaching steady state. Error bars, calculated from the standard deviation between the trajectory time-averages, are omitted for clarity, but are of a similar size to the symbols.

Appendix E. Spatial Segmental Orientation

The profiles of the segmental orientation per bond S_2^{xz} are calculated from a block-average after the system reaches equilibrium a steady state. The values are averaged along the z-coordinate using bins of 1 Å. The results Figure E.19 show that the molecular layers close to the surfaces are almost perfectly aligned with the sliding direction ($S_2^{xz} \approx 0.8$), in agreement with previous simulations [9, 49]. Further into the films there are oscillations in S_2^{xz} which correspond to the density oscillations in Figure 7.

Figure E.19: Profile of the segmental orientation, S_2^{xz}, as a function of the z coordinate during steady state sliding for two chain lengths: C_{16} and C_{60}. a) 0.5 GPa, 10 m s^{-1}, b) 0.5 GPa, 100 m s^{-1}, c) 1.5 GPa, 10 m s^{-1} and d) 1.5 GPa, 100 m s^{-1}

ACCEPTED MANUSCRIPT

- Large-scale (up to 50,000 atoms, 250 ns) nonequilibrium molecular dynamics simulations performed to investigate n-alkane behaviour under extreme conditions
- Longer n-alkanes show stronger layering and more long-range order, suggesting more solid-like films
- Longer n-alkanes give higher shear stress but a weaker shear rate dependence
- This behaviour can be partially attributed to both shear-induced melting and non-linear flow

ACCEPTED MANUSCRIPT